

RSC Advances



This is an *Accepted Manuscript*, which has been through the Royal Society of Chemistry peer review process and has been accepted for publication.

Accepted Manuscripts are published online shortly after acceptance, before technical editing, formatting and proof reading. Using this free service, authors can make their results available to the community, in citable form, before we publish the edited article. This *Accepted Manuscript* will be replaced by the edited, formatted and paginated article as soon as this is available.

You can find more information about *Accepted Manuscripts* in the [Information for Authors](#).

Please note that technical editing may introduce minor changes to the text and/or graphics, which may alter content. The journal's standard [Terms & Conditions](#) and the [Ethical guidelines](#) still apply. In no event shall the Royal Society of Chemistry be held responsible for any errors or omissions in this *Accepted Manuscript* or any consequences arising from the use of any information it contains.

ARTICLE

Metallohalide perovskite-polymer composite film for hybrid planar heterojunction solar cells

Cite this: DOI: 10.1039/x0xx00000x

Qifan Xue,[†] Zhicheng Hu,[†] Chen Sun, Ziming Chen, Fei Huang,^{*} Hin-Lap Yip,^{*} and Yong CaoReceived 00th January 2012,
Accepted 00th January 2012

DOI: 10.1039/x0xx00000x

www.rsc.org/

A polymer with tailored chemical functionality was introduced as a processing additive to control the film formation of the $\text{CH}_3\text{NH}_3\text{PbI}_3$ perovskite structure, leading to enhanced photovoltaic performance in a PEDOT:PSS/perovskite/PCBM-based planar heterojunction solar cell under optimized conditions. By adjusting the polymer doping content and the processing solvent, the grain size, film coverage and the optical properties of the perovskite films can be effectively tuned. At optimized conditions, the planar heterojunction solar cell composed of a thin layer of perovskite-polymer film (~50nm) exhibits an average PCE of 6.16% with a V_{oc} of 1.04 V, a J_{sc} of 8.85 mA/cm^2 and a FF of 0.65, which are much higher than those of the control device with a pristine perovskite film. The higher performance was attributed to improved morphology and interfaces of the perovskite-polymer films, which reduced the undesired contact between PEDOT:PSS and PCBM and minimized the shunting paths in the device. In addition, since the fabrication process for the perovskite solar cells can be performed at low temperature, flexible cells built on plastic substrate can therefore be realized with a PCE of 4.35%.

Introduction

Solar cells based on organometal trihalide perovskites (eg. $\text{CH}_3\text{NH}_3\text{PbI}_3$) as light absorbers are emerging as a low-cost and high performance photovoltaic technology that may fulfil the requirements for large-scale deployment of solar energy. Over the past few years, significant progress was made in perovskite solar cells with power conversion efficiencies (PCE) improved dramatically from 3% to over 15%.¹⁻¹¹ Recent studies revealed that organometal trihalide perovskites exhibit several desired properties for photovoltaic applications including facile tunable bandgaps,^{12,13} high absorption coefficient,¹³ long carrier-diffusion lengths,^{14,15} high ambipolar mobilities and low exciton binding energy,¹³ making them a very appealing class of material for new generation photovoltaic technology.

The perovskite semiconductors can also be adopted in various types of solar cell architectures including perovskite-sensitized solar cells, meso-superstructured solar cells and planar p-i-n heterojunction solar cells.¹⁻⁹ The latter is particularly attractive for potential commercialization due to the simplicity of the device structure, the low-temperature solution processibility and the

potential of large-scale manufacturing of the perovskite cells using a continuous coating technique on flexible substrates.^{8,16-18}

There are several issues that need to be addressed in order to improve the performance of planar heterojunction perovskite cells. First, interfacial materials with good charge selectivity are required to reduce interfacial charge recombination. In a typical p-i-n planar heterojunction structure, the perovskite thin film is sandwiched between a hole selective layer (eg. PEDOT:PSS) and an electron selective layer (eg. PCBM) while a transparent ITO-coated glass substrate and a low work function metal are used as anode and cathode, respectively. (Fig. 1a) This structure is advantageous as both the interlayers can be processed at low temperatures and also have proven processibility using large-area coating technique as demonstrated in roll-to-roll manufactured organic photovoltaic devices.²⁰⁻²³

Second, the quality of the perovskite films including the crystallinity, morphology and coverage also need to be optimized in order to improve the performance of the perovskite solar cells.^{20,24-28} Snaith *et al.* showed that the crystallization rate of perovskite films could be controlled using mixed halide such as $\text{CH}_3\text{NH}_3\text{PbI}_3$.

$x\text{Cl}_x$.^{29,30} Prolonging the crystallization and growth process in mixed halide perovskites provides better processing window to prepare good quality films with high coverage, which is crucial to improve the performance of the solar cells. Adding high boiling point solvent additive to the mixed halide perovskite solution also proved to be an efficient way to modulate the perovskite film morphology.²⁶ However, the relatively long annealing time and the difficulty in controlling the final stoichiometry are the drawbacks for the mixed halide perovskites.^{14,15,26}

$\text{CH}_3\text{NH}_3\text{PbI}_3$ is structurally more simple but it remains a challenge to control the crystallization process and the quality of the perovskite films.^{17,18,31} Although several methods including the use of mixed solvents,³² control of precursor concentration and film drying rate,^{17,31} and a novel two-step deposition process has been developed to improve the morphology and coverage of the $\text{CH}_3\text{NH}_3\text{PbI}_3$ films,^{8,33,7,34} there is still considerable room to further improve the perovskite solar cell performance by introducing a new processing strategy to effectively manipulate the perovskite film morphology.

In this work, a polymer additive with tailored chemical functionality was introduced into the $\text{CH}_3\text{NH}_3\text{PbI}_3$ perovskite structure to control the crystallization process and morphology of the perovskite films. The process-structure-performance relationships of the perovskite solar cells were studied. We found that the performance of the planar heterojunction perovskite solar cells with device structure of ITO/PEDOT:PSS/ $\text{CH}_3\text{NH}_3\text{PbI}_3$ Polymer/ $\text{PC}_{61}\text{BM}/\text{Al}$ (Fig. 1a and 1b) was strongly dependent on the choice of solvents and also the content of polymer additive in the perovskite precursor solutions. At optimized conditions, the best performing planar heterojunction solar cells composed of a thin layer of $\text{CH}_3\text{NH}_3\text{PbI}_3$ perovskite-polymer composite film (~50 nm) exhibits a PCE of 6.35% with a V_{oc} of 1.07 V, a J_{sc} of 8.95 mA/cm^2 and a FF of 0.66, which are much higher than those of the control device with a pristine perovskite film. In addition, by taking the advantage of low temperature processes required for the fabrication of the perovskite solar cells, we successfully demonstrated flexible cells on ITO-coated poly(ethylene terephthalate) (PET) substrates.

Experimental section

Materials:

Methylammonium iodide ($\text{CH}_3\text{NH}_3\text{I}$) was synthesized according to the reported procedure.⁵ To prepare the $\text{CH}_3\text{NH}_3\text{PbI}_3$, $\text{CH}_3\text{NH}_3\text{I}$ and PbI_2 , PbCl_2 (Alfa Aesar) were mixed in DMF or γ -butyrolactone (GBL) to form a 15 wt% solution at 60 °C overnight while being stirred in a glovebox with moisture and oxygen levels <1ppm. Poly(2-ethyl-2-oxazoline) (PEOXA, M.W 50k) was purchased from Alfa Aesar and used directly without further purification. [6,6]-Phenyl- C_{61} -butyric acid methyl ester (PC_{61}BM , Luminescence Technology Corp.) was dissolved in chlorobenzene (CB, Sigma-Aldrich).

Device fabrication and characterization:

The patterned ITO-coated glass and PET substrates were cleaned by sonication in detergent, deionized water, acetone and isopropyl alcohol subsequently and then dried under 80 °C in baking oven, followed by an oxygen plasma treatment for 4 min. A 40 nm thick poly(3,4-ethylenedioxythiophene) : poly(styrene sulfonate) (PEDOT:PSS, Clevios™ P VP AI 4083) was spun cast onto the ITO substrate and then dried at 120 °C for 20 min. The $\text{CH}_3\text{NH}_3\text{PbI}_3$:PEOXA precursor solution was then spun cast on the PEDOT:PSS layer resulted in a composite film with nominal thickness of ~ 50 nm. The film was then further annealed at 100 °C for 15 min to promote crystallization of the $\text{CH}_3\text{NH}_3\text{PbI}_3$ perovskite. Mixed halide $\text{CH}_3\text{NH}_3\text{PbI}_x\text{Cl}_{3-x}$ perovskite films with thickness of ~300 nm were prepared by spin coating the mixed solution of $\text{CH}_3\text{NH}_3\text{I}$ and PbCl_2 in DMF with a molar ratio of 3 : 1 and then annealed at 100 °C for 2h. To generate the bilayer, PC_{61}BM was spun cast onto the $\text{CH}_3\text{NH}_3\text{PbI}_3$ -PEOXA layer at 2000 rpm for 30 s. Finally, 100 nm of aluminium was thermally evaporated onto the substrates through a shadow mask at a base pressure of 1×10^{-6} mbar to complete the devices. The overlapping area between the cathode and anode defined the device area of 0.16 cm^2 .

Current density-voltage (J - V) characteristics for the devices were measured under 100 mW/cm^2 air mass 1.5 global (AM 1.5 G) illumination with a solar simulator (Oriel model 91192). The light intensity was calibrated using an National Renewable Energy Laboratory (NREL) calibrated silicon photodiode with a KG5 filter. UV-vis absorption and photoluminescence spectra were recorded on a HP 8453 spectrophotometer and FLS920 spectrofluorimeter (Edinburgh), respectively. The SEM images were obtained using a Zeiss EVO 18 scanning electron microscopy. Atom force microscopy (AFM) measurements were carried out using a Digital Instrumental DI Multimode Nanoscope IIIa in tapping mode. The crystal structure of $\text{CH}_3\text{NH}_3\text{PbI}_3$ -PEOXA films was investigated with an X-ray diffractometer (PANalytical X'pert PRO) equipped with a $\text{Cu-K}\alpha$ X-ray tube. With a scan angle of 1° and a step size of 0.04° as well as a time step of 3 s, we carried out the acquisition in the range of 10–60° in θ -2 θ mode.

Results and discussion

Selection principle for polymer additive

The selection criteria for the polymer additive is that it should contain chemical functionality that can form strong interactions with the $\text{CH}_3\text{NH}_3\text{PbI}_3$ structure in order to effectively tune the film formation kinetics. N,N -dimethylformamide (DMF) is the most commonly used solvent for processing the $\text{CH}_3\text{NH}_3\text{PbI}_3$ films as it provides strong interactions with the PbI_2 and $\text{CH}_3\text{NH}_3\text{I}$ precursors and hence results in a thoroughly mixed solution. Therefore, we selected poly(2-ethyl-2-oxazoline) (PEOXA) as the polymer additive as it contains an amide moiety in the polymer backbone which resembles the molecular structure of DMF and we hypothesize that PEOXA will strongly interact with

perovskite possibly through N-N interaction and hydrogen bonding (Fig.1a). Since PEOXA is an electrically insulating polymer, the content of PEOXA in the perovskite film should be carefully tuned to minimize its adverse effect on the electrical property of the solar cells. Another solvent that we had tested in conjunction with DMF is γ -butyrolactone (GBL), which is also a commonly used solvent for preparing $\text{CH}_3\text{NH}_3\text{PbI}_3$ films. It is worth noting that the solubility of $\text{CH}_3\text{NH}_3\text{PbI}_3$ in DMF is greater than that in GBL, which indicated that the interaction between the perovskite and GBL is weaker compared to that with DMF.

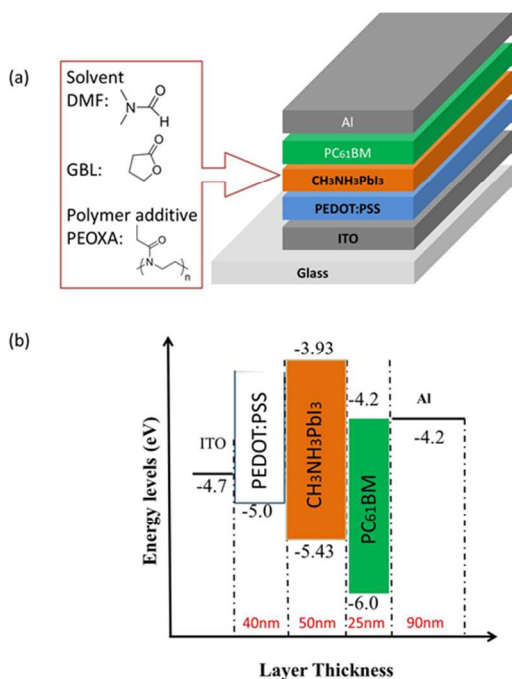


Figure.1 (a) Device structure of the hybrid planar heterojunction solar cell and the molecular structure of the solvents and polymer additive used in this study. (b) Schematic drawing of the energy levels and thickness of each layer in the device. The energy levels are taken from literature.^{15,16,25}

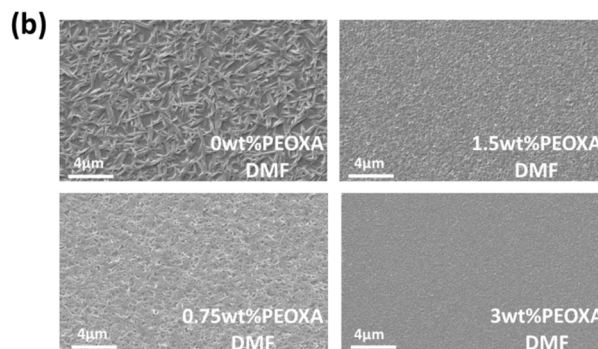
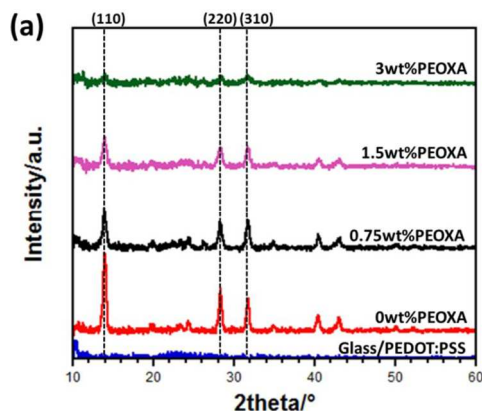
Table 1. The photovoltaic parameters of planar heterojunction solar cells based on the $\text{CH}_3\text{NH}_3\text{PbI}_3$ -PEOXA composite film prepared from DMF with the different doping content of PEOXA (0wt%, 0.75wt%, 1.5wt%) from a batch of 40 devices.

	V_{oc} (V)	J_{sc} (mA/cm ²)	FF(%)	PCE(%)
0wt%PEOXA	0.82 ± 0.03	7.78 ± 0.24	63.4 ± 1.2	4.21 ± 0.21
0.75wt%PEOXA	0.64 ± 0.01	4.46 ± 0.11	49.1 ± 1.9	1.43 ± 0.08
1.5wt%PEOXA	0.50 ± 0.01	4.02 ± 0.19	58.7 ± 2.3	1.14 ± 0.19

Perovskite film morphology and device characteristics prepared from DMF solvent

The pristine perovskite and perovskite/PEOXA composite films prepared from DMF solutions were first studied. X-ray diffraction (XRD) and scanning electron microscopy (SEM) were used to study the crystal structure and morphology of the films. The XRD patterns of the films are shown in Figure 2a. Pristine perovskite film shows strong peaks at $2\theta = 14.0^\circ$, 28.2° and 31.6° , which corresponds to the (110), (220) and (310) planes, respectively, indicating that the formation of tetragonal perovskite structure with lattice constants $a=b=8.883 \text{ \AA}$ and $c=12.677 \text{ \AA}$, which are consistent with the previously reported crystal structure.^{1,3,34-36}

With increasing content of PEOXA in the perovskite films, the XRD peak intensity of $\text{CH}_3\text{NH}_3\text{PbI}_3$ films decreased and the peaks were nearly completely diminished after adding 3wt% of PEOXA. However, the peak positions did not change with the PEOXA content, indicating that the crystal structure remained but only the crystallinity of the film decreased. SEM images revealed that the perovskite films deposited on PEDOT:PSS coated ITO appeared as a form of needle-like crystals randomly distributed on the surface. (Fig.2b). The crystals only partially covered the substrate leaving part of the PEDOT:PSS exposed. Upon adding the PEOXA, the film morphology became more uniform and the coverage increased. The needle-like crystals were also found to break down with increasing PEOXA doping and it became a featureless, smooth film when 3 wt% of PEOXA was added. The change of morphology upon PEOXA addition is in agreement with the XRD data as the crystallinity is decreased with increasing PEOXA content.



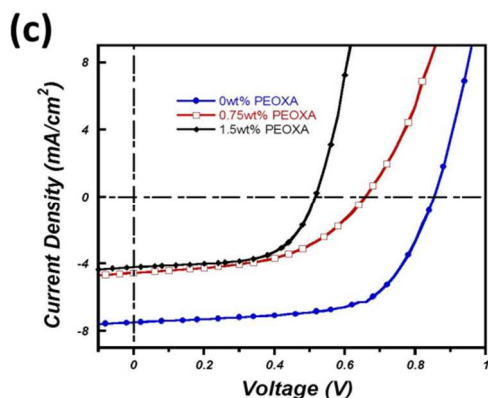


Figure 2. (a) X-ray diffraction patterns for $\text{CH}_3\text{NH}_3\text{PbI}_3$ -PEOXA films prepared from DMF solvent on glass/PEDOT:PSS substrate. (b) Scanning electron microscopy images of the $\text{CH}_3\text{NH}_3\text{PbI}_3$ -PEOXA films on ITO/PEDOT:PSS substrate. (c) Current density–Voltage (J - V) characteristics of the solar cells with the perovskite and perovskite-PEOXA films prepared from DMF.

Based on the trend observed by XRD and SEM, we conclude that PEOXA can interact strongly with the $\text{CH}_3\text{NH}_3\text{PbI}_3$ and significantly suppress the growth of the perovskite crystal.

To study the polymer additive effect on the performance of the perovskite solar cells, we fabricated perovskite/fullerene planar heterojunction solar cells based on the structure of ITO/PEDOT:PSS/Perovskite/PCBM/Al and the J - V curves and the performance parameters are shown in Fig. 2(c) and Table 1, respectively. The solar cells based on the pristine $\text{CH}_3\text{NH}_3\text{PbI}_3$ film processed from DMF delivered an average PCE of 4.21% with V_{oc} , J_{sc} and FF equal to 0.82 V, 7.78 mA/cm^2 and 0.634, respectively. These results are comparable to that in other reports with similar device structure.¹⁸ The device performance deteriorated with increasing content of PEOXA and the PCE dropped to ~1.5% with lost in all PV parameters. We attribute that to the breakdown of the $\text{CH}_3\text{NH}_3\text{PbI}_3$ perovskite structure. When the content of PEOXA increased to 3 wt%, no obvious photovoltaic effect could be observed in our solar cells due to the amorphous nature of the perovskite film.

Thicker perovskite films are typical required to achieve high J_{sc} . However, it is challenging to obtain smooth and thick $\text{CH}_3\text{NH}_3\text{PbI}_3$ films through one-step solution process as the crystal growth process of perovskite is difficult to control. A commonly used approach to overcome this problem is to use mixed halide perovskite such as $\text{CH}_3\text{NH}_3\text{PbI}_x\text{Cl}_{3-x}$, which allows to form relative thick and smooth film with enhanced light harvesting property. To study the effect of PEOXA doping on the thicker perovskite films, we introduced smaller amount of PEOXA into the $\text{CH}_3\text{NH}_3\text{PbI}_x\text{Cl}_{3-x}$ precursor solution with DMF as the solvent. The control device based on the 300 nm pristine mixed halide perovskite film showed an average PCE of 9.47% with V_{oc} , J_{sc} and FF equal to 0.90 V, 18.21 mA/cm^2 and 0.572, respectively. The devices with 0.25wt% PEOXA doping delivered a lower average PCE of 8.96% with V_{oc} , J_{sc} and FF equal to 0.87 V, 17.93 mA/cm^2 and 0.568 while the one doped with 0.75wt% PEOXA showed even lower performance.

(See supporting information: Table. S1, Fig. S2 and S3). These results are in good agreement with the $\text{CH}_3\text{NH}_3\text{PbI}_3$ -based devices. Encouragingly, the standard deviation of the PEOXA doping device performance was lower compared to the reference device.

Considering that the strong interactions among DMF, PEOXA and the perovskite will significantly suppress the crystal growth of the perovskite film, we therefore chose GBL as another processing solvent for our study aiming to reduce the interactions among the solvent, polymer and perovskite and provide better control over the microstructure of the films. In addition, from the environmental aspect, GBL is a less hazardous solvent compared to DMF as it can be biodegradable while DMF is much more toxic.

Perovskite film morphology, optical property and device characteristics prepared from GBL solvent

The pristine perovskite and perovskite/PEOXA composite films prepared from GBL were also characterized by XRD and SEM and the results are shown in Fig 4a and 4b, respectively. Similar to the case of the DMF-processed film, the pristine perovskite film showed strong peaks at $2\theta = 14.0^\circ$, 28.2° and 31.6° , revealing the perovskite formation. However, there was an additional peak found at 12.65° , which corresponded to a low level impurity of PbI_2 . Similar results were found in other reports when GBL was used as the processing solvent.^{17,18,31,33} We attribute the presence of the PbI_2 phase to its relatively low solubility in GBL and small amount of PbI_2 may exist in the precursor solution. When PEOXA was added, the intensity of the XRD peak of PbI_2 in the composite films decreased upon increasing loading of the polymer. When the concentration of polymer increased up to 3 wt% or higher, the PbI_2 peak totally diminished and only the perovskite phase visible in the film. The absence of PbI_2 suggests that PEOXA, with a molecular structure similar to that of DMF, can improve the solubility of PbI_2 and allows better mixing of the precursors in GBL solution. Another trend we observed is that with increasing content of PEOXA, the XRD peak intensity of $\text{CH}_3\text{NH}_3\text{PbI}_3$ films decreased steadily, which suggested that the crystal growth process was also suppressed. However, in the case of GBL-processed films, the perovskite peaks were still existed even at a 7 wt% polymer-doped film while they were totally vanished at only 3 wt% polymer-doped film when processed from DMF. We suggest that the majority of the polymer may form at the grain boundary of the perovskite crystals due to its strong interaction with the perovskite, however it is also likely that small portion of the polymer may also accumulate at the interfaces between the perovskite and the interlayers.

The SEM images of the perovskite films spun cast on ITO/PEDOT:PSS substrates are shown in Fig.3b. Different from the needle-like crystals observed in the DMF-processed films, the pristine $\text{CH}_3\text{NH}_3\text{PbI}_3$ film processed from GBL exhibited disk-like crystal structure with irregular shapes and very rough edges. The crystals were disconnected leaving a large portion of uncovered area with exposed PEDOT:PSS film. The average size of the crystal was about $2\mu\text{m}$. Upon adding the PEOXA additive, the crystal domains became more homogenous and the size of the crystals and also the average uncovered area decreased with increasing content of the PEOXA.

ARTICLE

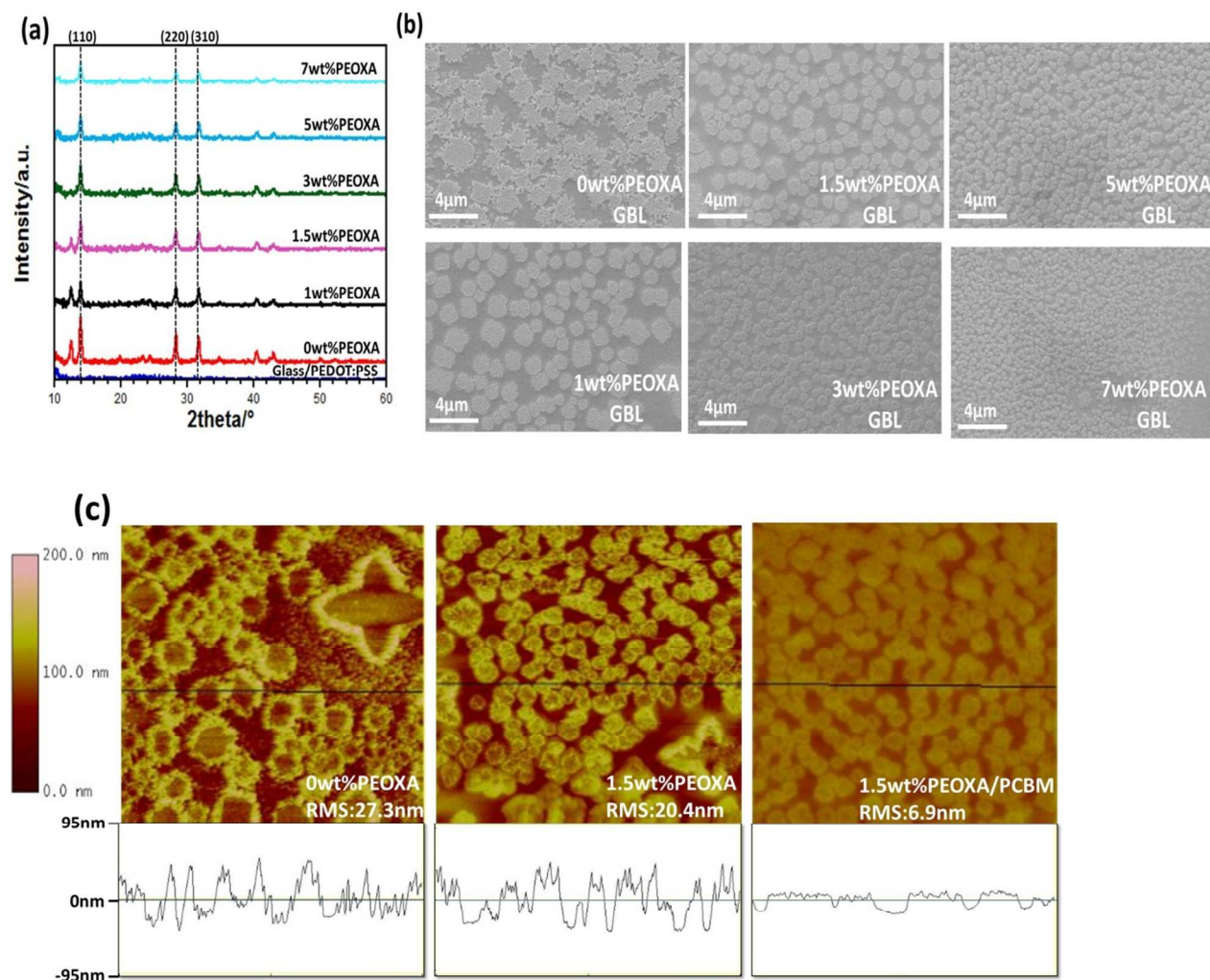


Figure 3. (a) XRD patterns for CH₃NH₃PbI₃-PEOXA films prepared from GBL on the glass/PEDOT:PSS substrate. (b) SEM images of the CH₃NH₃PbI₃-PEOXA films prepared from GBL on the ITO/PEDOT:PSS substrate. (c) AFM images and height profile for CH₃NH₃PbI₃-PEOXA films prepared from GBL with 0 wt% and 1.5wt% PEOXA and CH₃NH₃PbI₃-1.5wt% PEOXA /PC₆₁BM film on ITO/PEDOT:PSS substrates.. The scanning size of all the images is 20 μm × 20 μm.

The greater coverage of the CH₃NH₃PbI₃-PEOXA film may reduce the chance of direct contact between PC₆₁BM and PEDOT:PSS layer and minimize the shunting paths in the solar cells. To further evaluate the topography and the height profile of the perovskite-PEOXA films, atomic force microscopy (AFM) study were performed. (Fig.3c and Fig.S1). The surface of the pristine CH₃NH₃PbI₃ film was relatively rough, with the root-mean-square (RMS) roughness of 27.3 nm. Upon adding the polymer additive, the surface of the CH₃NH₃PbI₃-PEOXA composite films became smoother, with the RMS of 21.5, 20.4, 18.0, 16.7 and 9.9 nm for the films with 1 wt%, 1.5 wt%, 3 wt%, 5 wt% and 7 wt% of PEOXA,

respectively. (Fig.S1) The observed evolution of the morphology of the perovskite films from the AFM study is in good agreement with that observed by SEM. To further study how the PC₆₁BM film form on the perovskite films, we also studied the morphology of the PC₆₁BM film coated on the CH₃NH₃PbI₃-PEOXA(1.5 wt%) film as an example and the corresponding AFM image is shown in Fig 3c. Instead of forming a flat film, the 25 nm PC₆₁BM homogeneously coated on the composite film with surface topology replicated that of the underneath film but with a smaller RMS roughness of 6.9 nm. The good coverage of PC₆₁BM is important as it allows homojunction formation between the PC₆₁BM buffer layer and the

Al cathode and reduces the undesired contact between the perovskite film and the metal cathode.

The optical properties of the perovskite and composite films were studied and their absorption and photoluminescence (PL) spectra are shown in Fig 4a and 4b, respectively. A typical absorption spectrum for the pristine $\text{CH}_3\text{NH}_3\text{PbI}_3$ film was obtained with absorption edge at 780 nm, which corresponds to a bandgap of 1.50 eV and is consistent with previous reports.^{8,18,31} The absorbance of the perovskite films decreased with increasing content of the PEOXA, while the shape of the absorption curves remained the same. We attribute the decrease in absorbance to the reduced crystallinity of the perovskite in the composite films as observed from the XRD study. The steady-state PL study revealed a very interesting emission property of the studied films. The emission peak of the pristine $\text{CH}_3\text{NH}_3\text{PbI}_3$ film at ~ 780 nm was corresponding to the nanocrystalline perovskite particles as suggested by Choi *et al* and other reports.^{19,32,37,38} Highly crystalline bulk $\text{CH}_3\text{NH}_3\text{PbI}_3$ is a poor emitter with emission peak over 800 nm that we did not observe in our study.³⁷ Upon introduction of the PEOXA, a blue-shifted PL peak arose at 710 nm and this peak was increased with PEOXA content while the PL peak at 780 nm decreased accordingly. The feature peak at 710 nm has not been reported before and we attribute that to the emission from a more disordered perovskite phase resulted from the strong interaction with the PEOXA. The PL peak intensity at 710 nm increased with the PEOXA content is also in agreement with the fact that the emission property of the perovskite can enhance when the crystallinity decreased.³⁷⁻⁴⁰ It is worth noting that despite a distinct emission property was found in the composite films, the similarity in the absorption edge of those films indicated that there is an insignificant change in bandgap.

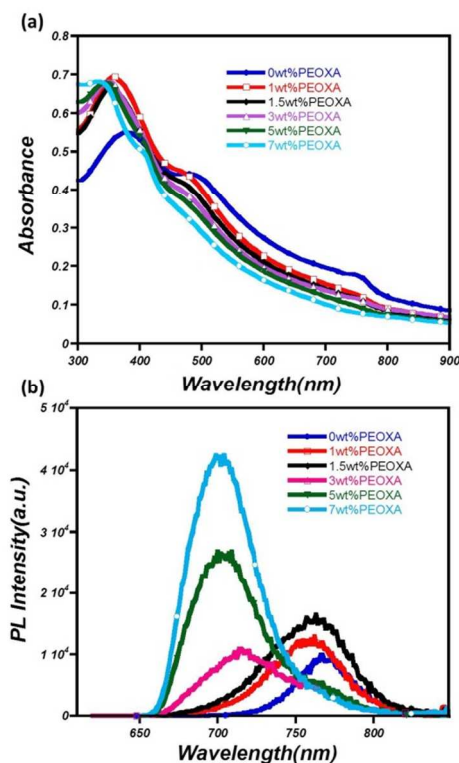


Figure.4 (a). UV-vis absorption spectra for quartz/ $\text{CH}_3\text{NH}_3\text{PbI}_3$ -PEOXA(50nm) with increasing the weight percent of PEOXA. (b). Photoluminescence spectroscopy for quartz/ $\text{CH}_3\text{NH}_3\text{PbI}_3$ -PEOXA(50nm) with increasing the weight percent of PEOXA ($\lambda_{\text{exc}}=610\text{nm}$).

The performances of the perovskite planar heterojunction solar cells processed from GBL are summarized in Table 2 and Fig 5. Solar cells based on the pristine $\text{CH}_3\text{NH}_3\text{PbI}_3$ perovskite film delivered a lower performance compared to that processed from DMF, with a V_{oc} of 0.71 V, a J_{sc} of 7.47 mA/cm^2 , a FF of 0.45 and a corresponding PCE of 2.37 %. We attribute the lower performance to the reduced coverage of the perovskite film and the presence of large amount of PbI_2 phase. However, when a small amount of PEOXA was introduced in the perovskite films, the performance of the solar cells significantly improved with all three photovoltaic parameters improving simultaneously at optimized conditions. In general, the V_{oc} of the devices with PEOXA doping is much higher than that from the pristine perovskite film. It increased with the PEOXA content reaching a maximum V_{oc} of 1.1 V at 3 and 5 wt% doping concentration before decreasing again at higher doping concentration. It is worth to note that typically the V_{oc} for the best solution-processed $\text{CH}_3\text{NH}_3\text{PbI}_3$ /PCBM planar heterojunction solar cells are only in the range of 0.8 - 0.9 V.^{17,18,31} A V_{oc} of 1.1V was only achieved in the high performance Al_2O_3 -based meso-structured perovskite solar cells and vapor-deposited perovskite solar cells.^{4-6,9,41} We attribute the improved V_{oc} not only to the higher coverage of the perovskite-polymer film, but also to the reduced number of contacts between PEDOT:PSS/PCBM as a thin layer of PEOXA may block the undesired PEDOT:PSS/PCBM contact which can act as a charge recombination site.¹¹ A little drop of the V_{oc} at the 7 wt% PEOXA-doped device may be due to the formation of a relatively thick insulating PEOXA layer at the device junction, forming a poor diode as revealed by the low FF of the device. Therefore, the strategy demonstrated here is an important means to further enhance the performance of perovskite/fullerene-based solar cells.

In addition to the improvement of V_{oc} , an increase in J_{sc} and FF were also found when an appropriate amount of PEOXA was added to the perovskite films. The J_{sc} increased from 7.47 mA/cm^2 in the pristine film to 8.95 mA/cm^2 at 1.5 wt% PEOXA doping and then plateaued at ~ 7 mA/cm^2 at higher wt% PEOXA doping before significantly dropping to ~ 2.5 mA/cm^2 at 7 wt% doping. The increase in J_{sc} cannot be simply explained by the absorption spectra of the films as the pristine film showed the largest absorbance. Therefore the improved charge generation and extraction at optimized perovskite/PEOXA film may account for the increase in J_{sc} . To study the spectral response of the different devices, The incident photon to electron conversion efficiency (IPCE) measurement was performed and the result are shown in Fig 5. The 1.5 wt% PEOXA doped devices showed a marked enhancement of the IPCE with a broad spectral response in the region from the visible to near-infrared and reached a peak of 48% at ~ 450 nm.

ARTICLE

Table 2 The photovoltaic parameters of planar heterojunction solar cells based on the $\text{CH}_3\text{NH}_3\text{PbI}_3$ -PEOXA composite film prepared from GBL with the different ratio of PEOXA (0wt%, 1wt%, 1.5wt%, 3wt%, 5wt%, 7wt%) from a batch of 40 devices.

	V_{oc} (V)	J_{sc} (mA/cm^2)	FF(%)	PCE(%)	R_s (Ωcm^2)	R_p (Ωcm^2)
0wt%PEOXA	0.68±0.02	7.27±0.13	42.4±2.1	2.13±0.28	25±4	380±30
1wt%PEOXA	0.90±0.03	7.54±0.38	66.5±1.7	4.65±0.31	13±2	1024±32
1.5wt%PEOXA	1.04±0.03	8.85±0.15	65.2±1.3	6.16±0.18	7±2	1328±101
3wt%PEOXA	1.08±0.01	6.69±0.12	60.3±2.5	4.49±0.15	16±3	968±120
5wt%PEOXA	1.09±0.01	6.87±0.22	50.5±4.6	4.12±0.12	22±2	1205±301
7wt%PEOXA	0.98±0.03	2.44±0.15	40.4±2.3	0.91±0.13	108±28	1009±185

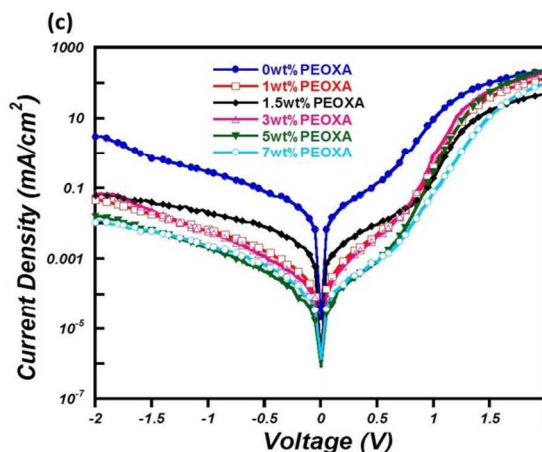
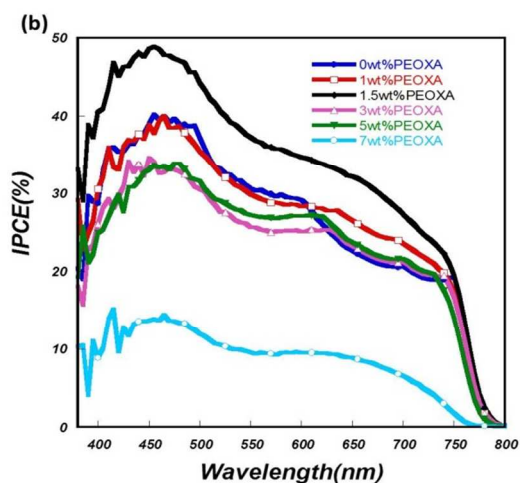
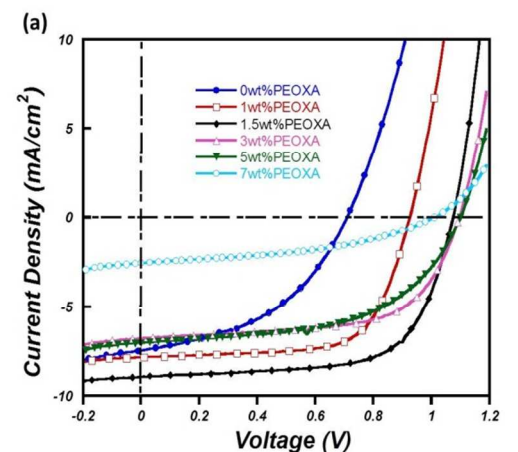


Figure 5 Current density–Voltage (J - V) characteristics for $\text{CH}_3\text{NH}_3\text{PbI}_3$ -PEOXA composite film with increasing the weight percent of PEOXA under 100mW m^{-2} air mass 1.5 global (AM 1.5 G) illumination (a) and in the dark (c). (b) IPCE spectra for $\text{CH}_3\text{NH}_3\text{PbI}_3$ -PEOXA composite film with increasing the weight percent of PEOXA.

Considering a relatively thin perovskite film with nominal thickness of ~ 50 nm was used, the J_{sc} and IPCE values are quite high indicating the perovskite is an excellent light absorber. The FF is another parameter that improved with the addition of PEOXA. The FF is governed by both the parasitic series resistance (R_s) and shunt resistance (R_p) of the solar cells.⁴²⁻⁴⁴ Typically R_s is determined by the bulk conductivity of the electrodes, active and interfacial layers, and the contact resistance between them while R_p is determined by the quality of the films and their interfaces. In our study the R_s and R_p were extracted by fitting the J - V curves with Lambert W function

to help to analyze the FF of different devices and the corresponding data are summarized in Table 2.^{42,43,45,46} When small amount of PEOXA was added, a high FF over 60% was achieved with both the R_s and R_p improved over the devices with pristine film. Taking the 1.5 wt% PEOXA doped devices as an example, a low R_s of $10 \Omega\text{cm}^2$ and a high R_p of $1468 \Omega\text{cm}^2$ were achieved while the pristine film showed a relatively high R_s of $29 \Omega\text{cm}^2$ and a lower R_p of $410 \Omega\text{cm}^2$. We suggest that despite a higher crystallinity found in the pristine film, the very rough edges of the irregular perovskite crystal domains as observed by the SEM study might act as charge scattering centers which affected the charge transport property of the film. While the well-defined crystal domains with smoother edges in the composite films could possess better charge transport properties and therefore accounts for the reduction of R_s . However, at very high PEOXA doping concentration the R_s of the corresponding devices were increased again due to the insulating property of the polymer additive.

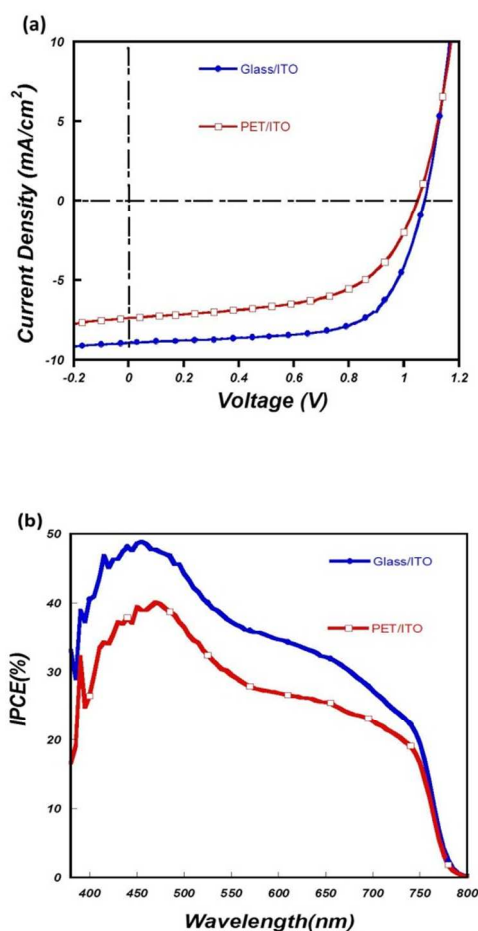


Figure.6 (a) Current density –Voltage (J - V) characteristics for $\text{CH}_3\text{NH}_3\text{PbI}_3$ -1.5wt%PEOXA composite film fabricated both on ITO-coated glass and PET under 100mW m^{-2} air mass 1.5 global (AM 1.5 G) illumination. (b) IPCE spectra for $\text{CH}_3\text{NH}_3\text{PbI}_3$ -1.5wt%PEOXA composite film fabricated both on ITO-coated glass and PET

Regarding to the R_p , we attribute the improvement of the composite films to the improved selective contact at the anode since a thin layer of PEOXA coated on the PEDOT:PSS could prevent it from directly contact with the PCBM through the uncovered void area of the perovskite film. It was previously reported that such a PEDOT:PSS/PCBM contact can form shunting paths not only affects the diode characteristic but also limits the V_{oc} of the perovskite solar cells.²⁹ The significant increase in the R_p suggested that the charge leaking at the anode interface was efficiently suppressed. The improved diode behavior of the PEOXA-doped devices can also be seen in the reduced dark current at the reversed bias region in the J - V plot as shown in Fig.5c, resulting in devices with better rectification and FF. With the simultaneous improvement in all the three device-related parameters, the best solar cell performance was achieved at the optimized 1.5wt% PEOXA doping showing a PCE up to 6.35% with a V_{oc} of 1.07 V, a J_{sc} of 8.95 mA/cm^2 and a FF of 0.66. It is also worth noting that the standard derivation of the device performance is lower when compared to other reported perovskite solar cells,^{5,8,16} indicating that the device reproducibility can be improved by employing a perovskite-polymer composite film.

Finally, taking advantage of the low temperature processes ($<150^\circ\text{C}$) required for the fabrication of the perovskite/fullerene planar heterojunction cells,^{16,47} we further demonstrated the possibility for making flexible devices on plastic substrates. Flexible hybrid planar heterojunction solar cells were fabricated on ITO-coated poly(ethylene terephthalate) (PET) substrates based on the optimal conditions ($\text{CH}_3\text{NH}_3\text{PbI}_3$ -1.5wt%PEOXA), giving a PCE of 4.35% with an V_{oc} of 1.05 V, a J_{sc} of 7.38 mA/cm^2 , a FF of 0.573 (Fig.6). Relative to the device performance based on the ITO-coated glass (PCE: 6.35%, V_{oc} : 1.07 V, J_{sc} : 8.95 mA/cm^2 , FF: 0.662), V_{oc} remain constant and the lower efficiency may be due to intrinsic limitations of PET plastic substrate including the lower optical transmittance (Fig. S7) and higher ITO sheet resistance ($60 \Omega \text{ sq}^{-1}$ vs. $15 \Omega \text{ sq}^{-1}$).

Conclusions

A polymer additive with tailored chemical functionality was introduced into the $\text{CH}_3\text{NH}_3\text{PbI}_3$ perovskite structure for the first time to control the morphology, electrical and optical properties of the perovskite films. At optimized conditions, the planar heterojunction solar cell composed of a thin layer of perovskite film ($\sim 50\text{nm}$) exhibits a PCE 6.35 % with a V_{oc} of 1.07 V, a J_{sc} of 8.95 mA/cm^2 and a FF of 0.66, which outperformed that of the devices with pristine perovskite film. Since the fabrication process for the perovskite solar cells can be performed at low temperature, flexible cells built on plastic substrates can therefore be realized with a PCE of 4.35%. We believed that the feasibility of using a chemically tailored additive to fine tune the properties of metalhalide perovskite films as demonstrated in this report provides a powerful means and new concept to further improve the performance of perovskite-based devices.

Acknowledgements

This work was financially supported by the Ministry of Science and Technology (No. 2014CB643505), the Natural Science Foundation of China (No. 51323003 and 21125419), and the Guangdong Natural Science Foundation (No. S2012030006232).

Notes and references

Institute of Polymer Optoelectronic Materials and Devices, State Key Laboratory of Luminescent Materials and Devices, South China University of Technology, Guangzhou 510640, P. R. China.

†These authors contributed equally to this work.

Electronic Supplementary Information (ESI) available: [details of any supplementary information available should be included here]. See DOI: 10.1039/b000000x/

- (1) Kojima, A.; Teshima, K.; Shirai, Y.; Miyasaka, T. *J. Am. Chem. Soc.* **2009**, *131*, 6050.
- (2) Kim, H.-S.; Lee, C.-R.; Im, J.-H.; Lee, K.-B.; Moehl, T.; Marchioro, A.; Moon, S.-J.; Humphry-Baker, R.; Yum, J.-H.; Moser, J. E.; Graetzel, M.; Park, N.-G. *Scientific Reports* **2012**, *2*, 591.
- (3) Im, J.-H.; Lee, C.-R.; Lee, J.-W.; Park, S.-W.; Park, N.-G. *Nanoscale* **2011**, *3*, 4088.
- (4) Lee, M. M.; Teuscher, J.; Miyasaka, T.; Murakami, T. N.; Snaith, H. J. *Science* **2012**, *338*, 643.
- (5) Ball, J. M.; Lee, M. M.; Hey, A.; Snaith, H. J. *Energy Environ. Sci.* **2013**, *6*, 1739.
- (6) Liu, M.; Johnston, M. B.; Snaith, H. J. *Nature* **2013**, *501*, 395.
- (7) Burschka, J.; Pellet, N.; Moon, S.-J.; Humphry-Baker, R.; Gao, P.; Nazeeruddin, M. K.; Graetzel, M. *Nature* **2013**, *499*, 316.
- (8) Liu, D.; Kelly, T. L. *Nature Photonics* **2014**, *8*, 133.
- (9) Wojciechowski, K.; Saliba, M.; Leijtens, T.; Abate, A.; Snaith, H. J. *Energy Environ. Sci.* **2014**, *7*, 1142.
- (10) He, M.; Zheng, D.; Wang, M.; Lin, C.; Lin, Z. *J. Mater. Chem. A* **2014**, *2*, 5994.
- (11) Wang, Q.; Dong, Q.; Xiao, Z.; Yuan, Y.; Huang, J. *Energy Environ. Sci.* **2014**, DOI: 10.1039/C4EE00233D.
- (12) Noh, J. H.; Im, S. H.; Heo, J. H.; Mandal, T. N.; Seok, S. I. *Nano Lett.* **2013**, *13*, 1764.
- (13) Stoumpos, C. C.; Malliakas, C. D.; Kanatzidis, M. G. *Inorg. Chem.* **2013**, *52*, 9019.
- (14) Stranks, S. D.; Eperon, G. E.; Grancini, G.; Menelaou, C.; Alcocer, M. J. P.; Leijtens, T.; Herz, L. M.; Petrozza, A.; Snaith, H. J. *Science* **2013**, *342*, 341.
- (15) Xing, G.; Mathews, N.; Sun, S.; Lim, S. S.; Lam, Y. M.; Graetzel, M.; Mhaisalkar, S.; Sum, T. C. *Science* **2013**, *342*, 344.
- (16) You, J.; Hong, Z.; Yang, Y.; Chen, Q.; Cai, M.; Song, T.-B.; Chen, C.-C.; Lu, S.; Liu, Y.; Zhou, H.; Yang, Y. *Acs Nano* **2014**, *8*, 1674.
- (17) Jeng, J.-Y.; Chiang, Y.-F.; Lee, M.-H.; Peng, S.-R.; Guo, T.-F.; Chen, P.; Wen, T.-C. *Adv. Mater.* **2013**, *25*, 3727.
- (18) Sun, S.; Salim, T.; Mathews, N.; Duchamp, M.; Boothroyd, C.; Xing, G.; Sum, T. C.; Lam, Y. M. *Energy Environ. Sci.* **2014**, *7*, 399.
- (19) Jin Hyuck, H.; Sang Hyuk, I.; Jun Hong, N.; Mandal, T. N.; Choong-Sun, L.; Jeong Ah, C.; Yong Hui, L.; Hi-jung, K.; Sarkar, A.; Nazeeruddin, M. K.; Gratzel, M.; Sang Il, S. *Nature Photonics* **2013**, *7*, 486.
- (20) Zuo, C.; Ding, L. *Nanoscale* **2014**, *6*, 9935.
- (21) Lin, Y.; Dam, H. F.; Andersen, T. R.; Bundgaard, E.; Fu, W.; Chen, H.; Krebs, F. C.; Zhan, X. *J. Mater. Chem. C* **2013**, *1*, 8007.
- (22) Kumar, M. H.; Yantara, N.; Dharani, S.; Graetzel, M.; Mhaisalkar, S.; Boix, P. P.; Mathews, N. *Chem. Commun.* **2013**, *49*, 11089.
- (23) Wu, H.; Zhao, B.; He, Z.; Yun, M.; Wang, M.; Huang, X.; Wu, J.; Cao, Y. *J. Mater. Chem. C* **2014**, DOI: 10.1039/C3TC32520B.
- (24) Pellet, N.; Gao, P.; Gregori, G.; Yang, T. Y.; Nazeeruddin, M. K.; Maier, J.; Gratzel, M. *Angew Chem Int Ed Engl* **2014**, *53*, 3151.
- (25) Ogomi, Y.; Morita, A.; Tsukamoto, S.; Saitho, T.; Fujikawa, N.; Shen, Q.; Toyoda, T.; Yoshino, K.; Pandey, S. S.; Ma, T.; Hayase, S. *J. Phys. Chem. Lett.* **2014**, *1004*, 250.
- (26) Liang, P.-W.; Liao, C.-Y.; Chueh, C.-C.; Zuo, F.; Williams, S. T.; Xin, X.-K.; Lin, J.; Jen, A. K. Y. *Adv. Mater.* **2014**, DOI: 10.1002/adma.201400231.
- (27) Edri, E.; Kirmayer, S.; Mukhopadhyay, S.; Gartsman, K.; Hodes, G.; Cahen, D. *Nature communications* **2014**, *5*, 3461.
- (28) Colella, S.; Mosconi, E.; Fedeli, P.; Listorti, A.; Gazza, F.; Orlandi, F.; Ferro, P.; Besagni, T.; Rizzo, A.; Calestani, G.; Gigli, G.; De Angelis, F.; Mosca, R. *Chem. Mater.* **2013**, *25*, 4613.
- (29) Eperon, G. E.; Burlakov, V. M.; Docampo, P.; Goriely, A.; Snaith, H. J. *Adv. Funct. Mater.* **2014**, *24*, 151.
- (30) Snaith, H. J. *J. Phys. Chem. Lett.* **2013**, *4*, 3623.
- (31) Jeng, J. Y.; Chen, K. C.; Chiang, T. Y.; Lin, P. Y.; Tsai, T. D.; Chang, Y. C.; Guo, T. F.; Chen, P.; Wen, T. C.; Hsu, Y. *J. Adv. Mater.* **2014**, DOI: 10.1002/adma.201306217.
- (32) Kim, H.-B.; Choi, H.; Jeong, J.; Kim, S.; Walker, B.; Song, S.; Kim, J. Y. *Nanoscale* **2014**, DOI: 10.1039/C4NR00130C.
- (33) Chen, Q.; Zhou, H.; Hong, Z.; Luo, S.; Duan, H.-S.; Wang, H.-H.; Liu, Y.; Li, G.; Yang, Y. *J. Am. Chem. Soc.* **2014**, *136*, 622.
- (34) Bi, D.; Moon, S.-J.; Haggman, L.; Boschloo, G.; Yang, L.; Johansson, E. M. J.; Nazeeruddin, M. K.; Graetzel, M.; Hagfeldt, A. *Rsc Advances* **2013**, *3*, 18762.
- (35) Zhao, Y.; Nardes, A. M.; Zhu, K. *J. Phys. Chem. Lett.* **2014**, *5*, 490.
- (36) Park, N.-G. *J. Phys. Chem. Lett.* **2013**, *4*, 2423.
- (37) Choi, J. J.; Yang, X.; Norman, Z. M.; Billinge, S. J. L.; Owen, J. S. *Nano Lett.* **2014**, *14*, 127.
- (38) Roiati, V.; Mosconi, E.; Listorti, A.; Colella, S.; Gigli, G.; De Angelis, F. *Nano Lett.* **2014**, *14*, 2168.
- (39) Xue, Q.; Sun, C.; Hu, Z.; Huang, F.; Yip, H.-L.; Cao, Y. *Acta Chim. Sinica* **2014**, DOI: 10.6023/A14090674.
- (40) Xue, Q.; Hu, Z.; Liu, J.; Lin, J.; Sun, C.; Chen, Z.; Duan, C.; Wang, J.; Liao, C.; Lau, W. M.; Huang, F.; Yip, H.-L.; Cao, Y. *J. Mater. Chem. A* **2014**, *2*, 19598.
- (41) Abrusci, A.; Stranks, S. D.; Docampo, P.; Yip, H.-L.; Jen, A. K. Y.; Snaith, H. J. *Nano Lett.* **2013**, *13*, 3124.
- (42) Ding, J.; Radhakrishnan, R. *Solar Energy Materials and Solar Cells* **2008**, *92*, 1566.
- (43) Blom, P. W. M.; Mihailetschi, V. D.; Koster, L. J. A.; Markov, D. E. *Adv. Mater.* **2007**, *19*, 1551.
- (44) Yip, H.-L.; Jen, A. K. Y. *Energy Environ. Sci.* **2012**, *5*, 5994.

(45) Jain, A.; Kapoor, A. *Solar Energy Materials and Solar Cells*

2005, *86*, 197.

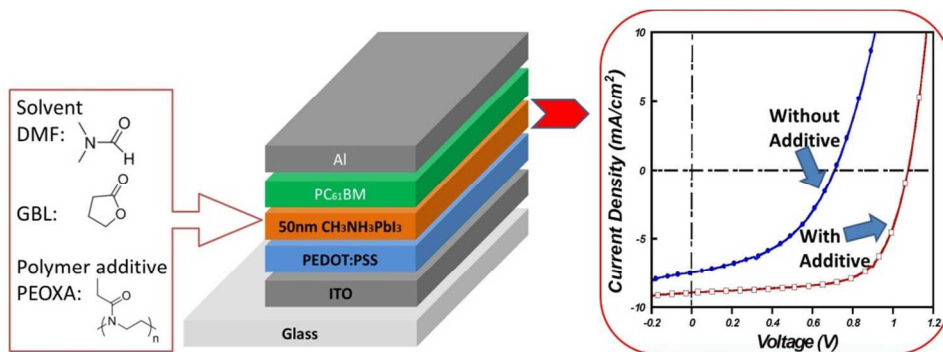
(46) Zhang, C.; Zhang, J.; Hao, Y.; Lin, Z.; Zhu, C. *J. Appl.*

Phys. **2011**, *110*, 504.

(47) Docampo, P.; Ball, J. M.; Darwich, M.; Eperon, G. E.; Snaith,

H. J. *Nature Communications* **2013**, *4*, 1.

TOC graph



Journal Name

RSCPublishing

ARTICLE

RSC Advances Accepted Manuscript